Acoustic Streaming Generated by Sharp Edges: The Coupled Influences of Liquid Viscosity and Acoustic Frequency

Chuanyu Zhang [1],* , **Xiaofeng Guo [1,2]** , **Laurent Royon [1]** and **Philippe Brunet [3],***

[1] Laboratoire Interdisciplinaire des Energies de Demain, Université de Paris; UMR 8236 CNRS, F-75013 Paris, France; xiaofeng.guo@esiee.fr (X.G.); laurent.royon@univ-paris-diderot.fr (L.R.)

[2] ESIEE Paris, Université Gustave Eiffel; F-93162 Noisy le Grand, France

[3] Laboratoire Matière et Systèmes Complexes, Université de Paris; UMR 7057 CNRS, F-75013 Paris, France

* Correspondence: chuanyu.dream@gmail.com (C.Z.); philippe.brunet@univ-paris-diderot.fr (P.B.); Tel.: +33-157276272 (P.B.)

check for updates

Abstract: Acoustic streaming can be generated around sharp structures, even when the acoustic wavelength is much larger than the vessel size. This sharp-edge streaming can be relatively intense, owing to the strongly focused inertial effect experienced by the acoustic flow near the tip. We conducted experiments with particle image velocimetry to quantify this streaming flow through the influence of liquid viscosity ν, from 1 mm^2/s to 30 mm^2/s, and acoustic frequency f from 500 Hz to 3500 Hz. Both quantities supposedly influence the thickness of the viscous boundary layer $\delta = \left(\frac{\nu}{\pi f}\right)^{1/2}$. For all situations, the streaming flow appears as a main central jet from the tip, generating two lateral vortices beside the tip and outside the boundary layer. As a characteristic streaming velocity, the maximal velocity is located at a distance of δ from the tip, and it increases as the square of the acoustic velocity. We then provide empirical scaling laws to quantify the influence of ν and f on the streaming velocity. Globally, the streaming velocity is dramatically weakened by a higher viscosity, whereas the flow pattern and the disturbance distance remain similar regardless of viscosity. Besides viscosity, the frequency also strongly influences the maximal streaming velocity.

Keywords: acoustofluidics; microfluidics; acoustic streaming; sharp edge; particle image velocimetry

1. Introduction

Acoustic streaming (AS) denotes the steady flow generated by an acoustic field in a fluid. Mathematically, it can be explained by the nonlinear coupling between acoustic wave and hydrodynamic momentum conservation equations. Physically, the underlying mechanism of AS comes from the dissipation of acoustic energy within the fluid, which induces spatial gradient of momentum, and in turn creates a time-averaged effective forcing [1–10].

The phenomenon has attracted researcher's attention since Faraday's observations in 1831 [11], who reported that light particles on vibrating plates spontaneously form steady clusters. More recently and especially in the context of microfluidics, AS has been proven to be a suitable technique for fluid and particle handling in various situations [4]. We wish to point out the studies on fluid mixing at a low-Reynolds number [12], particle manipulation and sorting [13–18], particle patterning [19,20] and heat transfer [21,22], among others.

Amongst different sorts of acoustic streaming, the one relevant in microfluidics situations usually involves viscous stress along walls or obstacles, generated by no-slip conditions and resulting in the presence of a viscous boundary layer (VBL). It is referred to *Rayleigh–Schlichting*

streaming [4,6–10], and is different from that induced by acoustic attenuation in the bulk of fluid. The bulk acoustic streaming is denoted as *Eckart streaming* [2,5] and becomes significant only with high frequencies (>MHz) or with very viscous liquids, so that the attenuation length is smaller than— or of the same order as—the vessel size [23–25]. In Rayleigh–Schlichting streaming, a non-zero, time-averaged vorticity is generated inside the unsteady VBL [7] of typical thickness $\delta = \left(\frac{2\nu}{\omega}\right)^{\frac{1}{2}}$, where ν is the kinematic viscosity and $\omega = 2\pi f$ the acoustic angular frequency. This vorticity appears in the form of an array of eddies pairs [6,7,10], denoted as inner vortices, along the channel walls [16,26,27]. This vorticity extends its influence beyond the VBL and in turn induces larger-scale eddies of width $\lambda/2$ [26,28] in the fluid bulk, where $\lambda = \frac{c_s}{f}$ is the acoustic wavelength and c_s the speed of sound. Rayleigh–Schlichting streaming is generally treated within the incompressibility framework.

Traditional acoustic streaming in microchannels is achieved by adjusting the channel width w and the wavelength λ to ensure a resonance condition, typically obtained when $w \simeq \lambda/2$ [29]. However, recent studies evidenced that relatively intense streaming could be generated by designing microchannels with sharp structures along the walls [30–36] excited by acoustic waves. The sharp structures can be easily prototyped by the facilities offered by microfabrication in clean rooms; e.g., with photolithography. One of the main advantages of "sharp-edge streaming" is that it can be generated at relatively low frequencies, typically in a range between a few hundred Hz and several kHz (but it is observed for much higher frequencies as well [34]). Within this low frequency range, numerous performant and stable piezoelectric transducers are available at low cost, and can be supplied with inexpensive amplifiers. Other advantages of operating at relatively low frequency include: efficient acoustic coupling between the transducer and the solid in contact, and negligible acoustic dissipation within the liquid. Finally, previous experiments reported that near the tip of the sharp edge, the streaming velocity can be very strong [30–32,37], and can even be comparable to the vibration velocity, hence up to several hundreds of mm/s [35,36] at a typical distance δ from the tip. Benefiting from these strong disturbances within the fluid inside a microchannel, various applications using sharp structures streaming have been developed: mixing processes [32,38], bio-particle control [39,40] and various on-chip devices [31,41].

The present study aims to investigate the influence of both liquid kinematic viscosity ν and acoustic frequency f on the streaming flow magnitude and pattern. The focus of this study is based on the fact that one of the key parameters of sharp-edge streaming is the thickness of the VBL, which depends on both f and ν. Actually, three main dimensionless numbers involve δ: the ratio of the tip diameter and δ, $d^* = \frac{2r_c}{\delta}$, the ratio with respect to the channel depth p, $p^* = \frac{p}{\delta}$ and the ratio between the channel width w and δ, $w^* = \frac{w}{\delta}$. Sharp-edge streaming is defined by the *sharpness* condition $d^* < 1$ [37], and almost no streaming could be noticed, even at relatively high forcing when $d^* \gg 1$ [35,36]. In the typical framework with water and f of a few kHz (let us say between 2500 and 6000 Hz as in previous studies), δ ranges between 7.3 and 11.3 µm, so that the two other ratios $w^*, p^* \gg 1$, for microfluidic channels, are typically thicker than 50 µm.

Additionally, quantifying the influence of viscosity distinguishes sharp edge acoustic streaming from classical ones. In classical Rayleigh–Schlichting streaming, the flow is found to be independent on viscosity providing that the VBL thickness δ is much thinner than the vessel size [8,9,42]. For sharp-edge streaming in microchannels or in wider vessels, it is found that this independence on viscosity is lost even if δ remains thin compared to the channel width w or depth p [37]. Ovchinnikov et al.'s perturbative theory predicts a decrease of the typical streaming velocity V_s with ν, though with a subtle dependence on the sharp-edge geometry. With a viscous enough liquid and/or a low enough frequency, the dimensionless lengths p^* or w^* can fall into the order of one. Under this condition, an overlap between geometrical confinement and the intrinsic nature of sharp-edge streaming makes it more complex to determine the influence of ν and f on the flow. On this latter point, Equation (22) from [37] predicted a typical streaming velocity in cylindrical coordinate (r, ϕ) as:

$$V_s(r) = \frac{V_a^2}{\nu} \frac{\delta^{2n-1}}{h^{2n-2}} H_\alpha\left(\frac{r}{\delta}\right) \tag{1}$$

where V_a is the amplitude of the acoustic velocity, n is a coefficient that depends on α as $n = \frac{\pi}{2\pi - \alpha}$; h is the length scale of the sharp-edge height. The function $H_\alpha\left(\frac{r}{\delta}\right)$ contains the radial profile of the streaming flow. It is worth noticing that Equation (1), supposedly valid in the range $r_c < \delta$, does not exhibit any dependence on r_c.

The present study intends to quantify the coupled role of viscosity and excitation frequency in both the streaming flow pattern and magnitude. The paper is organised as follows: Section 2 described the experimental setup and visualisation method. Then in Sections 3 and 4 the results at different viscosities and different frequencies are presented respectively. Finally, Section 5 summarises the main results and conclusions. The main physical quantities are defined in Table 1.

Table 1. Definition of the main physical quantities.

Quantity	Abbreviation
Kinematic viscosity	ν
Viscous boundary layer thickness	δ
Tip angle of sharp edge	α
Height of the sharp edge	h
Radius of curvature of the tip	r_c
Width of the microchannel	w
Depth of the microchannel	p
Acoustic frequency	f
Acoustic angular frequency	ω
Amplitude of acoustic displacement	$\mathbf{A}$
Amplitude of acoustic velocity	$\mathbf{V}_a$
Amplitude of acoustic velocity far from the tip	V_a
Streaming velocity	$\mathbf{V}_s$
Maximum streaming velocity	V_{smax}
Fitting coefficient relating V_{smax} and V_a^2	θ

2. Experimental Setup

2.1. Microchannel and Acoustic Wave

The experimental setup is sketched in Figure 1, and presented in more detail in [35]. It is built around a Y-shaped polydimethylsiloxane (PDMS) microchannel devised by standard photolithography techniques: starting from a SU8 resist-made mould of thickness 50 μm made on a silicon wafer, a mixture of PDMS (Sylgard 184) with 10% in mass of curing agent is poured on the SU8 mould and forms a 2.5-mm-thick layer on top of the wafer. After a baking at 65 °C for 4 h, the PDMS mixture is then sealed and attached to a glass coverslip after a 1 mn O_2 plasma treatment of both faces. A PDMS microchannel of depth $p = 50$ μm is then obtained. The width w is equal to 500 μm. Its geometrical dimensions are detailed in Figure 2a. Sharp edges with different angles (30°, 60°, 80° and 90°) could be fabricated from various moulds, and previous studies evidenced that a sharper tip and more acute angle would lead to stronger streaming under the same forcing amplitude [30–32,35,36]. For the present study, since the focus is on the influence of ν and f, we operated with the same angle of $\alpha = 60°$, with a corresponding tip diameter of $2r_c = 5.8 \pm 0.4$ μm.
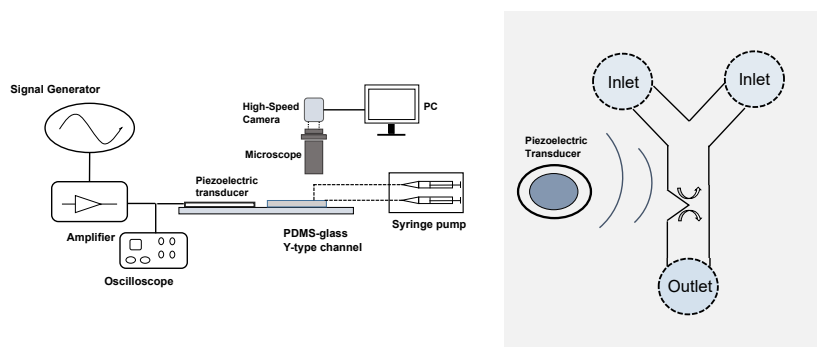
Figure 1. Left—Sketch of the experimental setup. A piezoelectric transducer is glued on a glass microscope slide, which is used as a coverslip for a PDMS microchannel with one or several sharp-edge structures. The transducer is supplied with a function generator and a home-made amplifier, adjusted by the peak-to-peak voltage monitored with an oscilloscope. The fluid seeded with fluorescent particles is brought by a syringe pump through two inlets. The flow inside the microchannel is visualised by a high-speed camera connected to a binocular microscope. Right —The piezo-transducer generates an acoustic wave within the Y-shaped channel. In the vicinity of the sharp-edge structure, the acoustic wave generates a streaming flow.
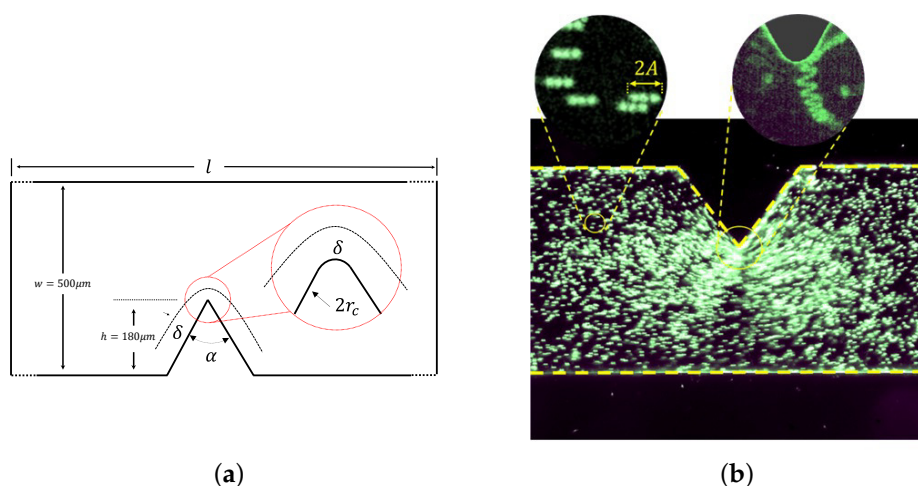

(**a**)   (**b**)

Figure 2. (**a**) Geometry of the microchannel and sharp-edge. (**b**) Trajectories of individual particles (diameter 4.9 µm), over several periods, for the left-hand-side zoom-in image. The frame per second (fps) equals $4f$ = 10,000 fps; for the right-hand-side one, the fps equals $10f$ = 25,000 fps; the two images have the same exposure time $1/(10f)$ = 1/25,000 s. Far from the tip, the flow is oscillating at frequency f and amplitude A, as testified by the segment described by each particle. Close to the tip, the trajectories of the particles show a superposition of oscillations with higher amplitude due to the sharp edge and advection due to the intense streaming flow.

The microchannel is fed with liquid seeded with fluorescent and reflective particles (green polystyrene microspheres, Thermo Scientific, Boston, MA, USA) of diameter 1 µm (The particle diameter has to be much smaller than δ to get the inner streaming flow, but to measure the amplitude of acoustic vibration velocity and get a qualitative image of the flow (see Figure 2b), larger particles of diameter 4.9 µm were more adapted) by a syringe pump (Newtown Company and Co, Newtown Blvd, Cebu). The acoustic wave is ensured by a piezoelectric transducer (Model ABT-455-RC, RS Components) glued on an upper glass microscope coverslip (width × length × thickness: 26 mm × 76 mm × 1 mm) with epoxy resist. The power is brought by a function generator (Model 33220A, Agilent, Santa Clara, CA, USA) with a home-made power amplifier. The transducer spectral response shows several resonance peaks between 400 and 40,000 Hz, from which we chose several values of

frequency from 500 to 3500 Hz. The applied voltage is sinusoidal, within a range between 0 and 60 V peak-to-peak (up to $\pm$ 30 V).

The fluids are mixtures of water (W) and glycerin (G) with different rate in W/G. Table 2 presents the main physical properties of different mixtures used in this study and the values of δ for the two extreme values of frequency.

Table 2. Physical properties of water-glycerol mixtures at 20 °C for different mass fraction $w_{\texttt{glyc}}$ and volume fraction $x_{\texttt{glyc}}$ of glycerol. Data for the viscosity ν of the water–glycerol mixture are extracted from [43], while the sound speed c_0 (at 25 °C) and the density ρ_0 are extracted from [44]. Additionally indicated are values of the VBL thickness δ at the highest and lowest frequency f, 3500 and 500 Hz.

$w_{\texttt{glyc.}}$	$x_{\texttt{glyc.}}$	ν (mm^2/s)	c_0 (m/s)	ρ_0 (kg/m^3)	δ_{3500} (µm)	δ_{500} (µm)
0.00	0.00	1.007	1510	998	9.57	25.3
0.062	0.05	1.158	1580	1012,7	10.3	27.1
0.457	0.4	4.32	1760	1114.5	19.8	52.4
0.654	0.6	13.75	1810	1168.3	35.4	93.6
0.747	0.7	29.44	1840	1193.4	51.7	136.9

2.2. Flow Visualisation and Image Processing

The visualisation is ensured by a fast camera (MotionBLITZ Cube4, Mikrotron) adapted on a binocular microscope. The depth of field of the microscope lens is about 10 µm, and hence five times smaller than the channel depth (p = 50 µm) which, after careful adjustments, enables one to access the streaming velocity near the centre plane. A cold-light beam shines from the bottom of the glass slide. While the seeded particles are fluorescent (excitation wavelength 480 nm, light emission wavelength 515 nm), we found that under some conditions of lighting, and due to the limited sensitivity of the camera, the diffused light could offer better contrast than the fluorescence-emitted light.

By operating under various exposure times and a frame-rate from 500 fps to 25,000 fps (see details in [35]), we can access both the steady streaming velocity $\mathbf{V}_s(x, y)$ and the acoustic velocity $\mathbf{V}_a(x, y) = \mathbf{A}\omega$ (via the vibration amplitude $\mathbf{A}$); see Figure 2. In particular, it is observed that close to the tip, $\mathbf{V}_s$ can be of the same order as $\mathbf{V}_a$. Far from the tip, where the streaming velocity vanishes, the time-cumulated trajectories of individual particles appear as straight segments, along the parallel direction with respect to the channel wall. The measurements of the lengths of these segments, equal to 2A, allow one to determine the prescribed vibration at infinity $V_a(\infty)$. This appears to us as the most reliable way to quantitatively measure the forcing amplitude, and we denote thereafter for simplicity: $V_a = V_a(\infty)$. As previously shown [35], the relationship between the prescribed voltage V and the vibration velocity V_a is found to be linear over the range 0–60 Volts. For each tested frequency, we proceeded a calibration between voltage and acoustic velocity.

The obtained images are treated with the open-source software ImageJ (https://imagej.net/). The streaming velocity field in the plane (x, y) is determined from the relative displacement of particles at a given phase during several vibration periods. Successive frames are converted into displacement vectors and vorticity maps by the software PIVlab (see: https://pivlab.blogspot.com/).

3. Influence of Viscosity

3.1. Velocity and Vorticity Maps

Figure 3a–d present typical streaming velocity fields obtained from the PIV treatment. The streaming flow appears as a main central jet from the tip, which is symmetric with respect to the y axis ($x = 0$). It clearly appears that the flow intensity decreases with an increasing viscosity. The jet induces the formation of two symmetric vortices beside the sharp edge. In terms of location,

the eddies are very near to the tip for the lowest viscosity, and for more viscous liquids they are pushed away and more aside from the tip. Let us also remark that at higher viscosity (Figure 3c,d), the flow in the VBL along the lateral walls becomes relatively thicker.
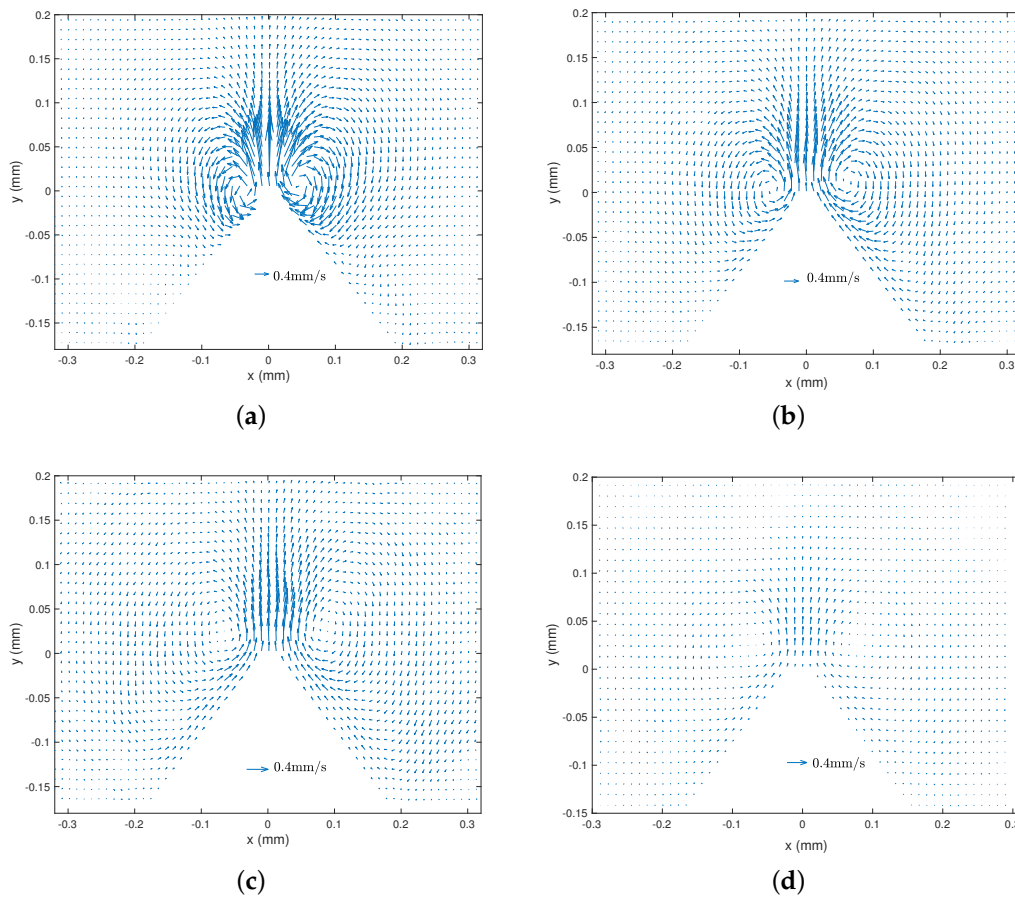

Figure 3. Streaming velocity field $V_s(x,y)$ from PIV measurements, with different liquid viscosities. f = 2500 Hz and V_a = 35 mm/s. (**a**) ν = 1.158 mm^2/s, (**b**) ν = 4.32 mm^2/s, (**c**) ν = 13.75 mm^2/s, (**d**) ν = 29.44 mm^2/s. Scales are the same for the four cases.

Figure 4 shows the vorticity maps corresponding to the fields of Figure 3. The most remarkable point is the decrease of the intensity of the vorticity with increasing viscosity, as testified by the scales of the colourmaps from (a) to (d). However, the size of the vortices, which may characterise the disturbance distance, remains roughly equal for all liquid samples. Additionally, the thickness of the inner vorticity areas, and the absolute vorticity within this specific region appear to be roughly constant for all liquids.
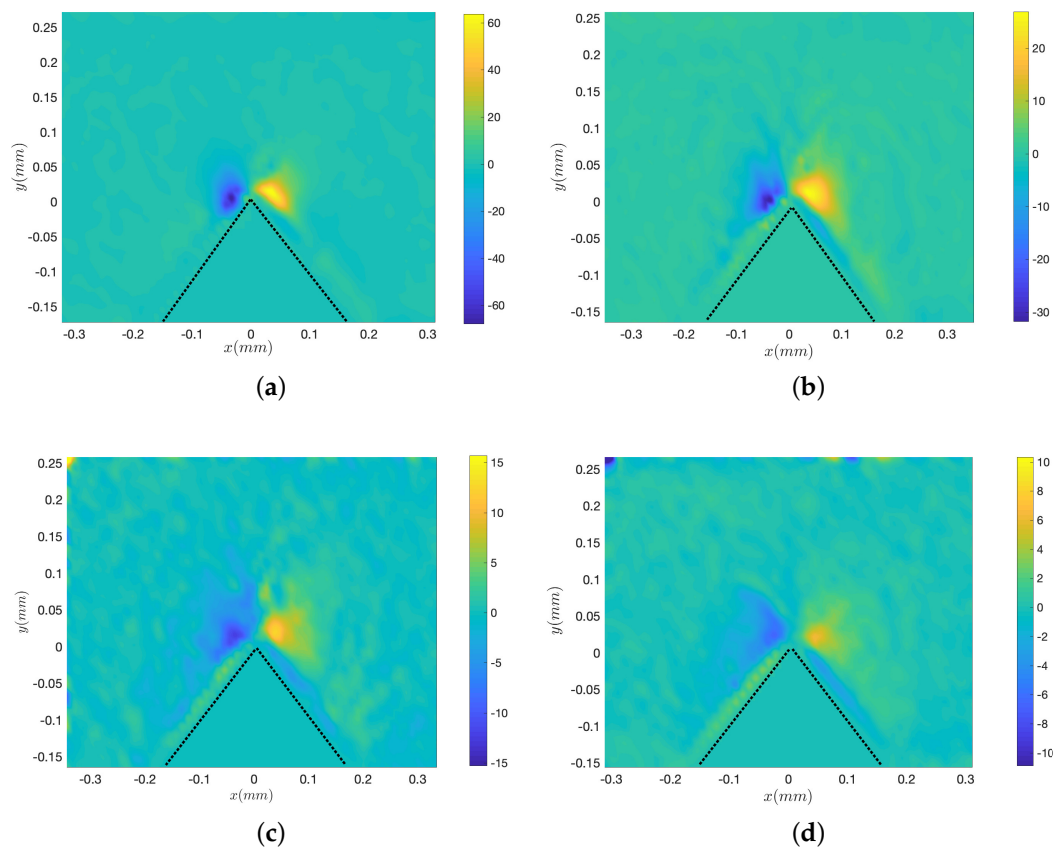
Figure 4. Vorticity maps of the streaming fields corresponding to the cases of Figure 3a–d, with corresponding colour bars that emphasise the decrease of vorticity. f = 2500 Hz and V_a = 35 mm/s. (**a**) ν = 1.158 mm^2/s, (**b**) ν = 4.32 mm^2/s, (**c**) ν = 13.75 mm^2/s, (**d**) ν = 29.44 mm^2/s. Dotted lines show the boundaries of the sharp edge.

3.2. Maximal Streaming Velocity at Different Viscosities

To further quantify the flow pattern, we extract the flow profile along the y axis: $V_s(x = 0, y)$, for different viscosities and forcing amplitudes. Figure 5 shows three examples of profiles for the same V_a = 35 mm/s and Fluids 2, 3 and 4 (see Table 2). It shows a quantitative confirmation that a higher viscosity entrains less intense and relatively more spread profiles. Since the velocity fields are symmetrical with respect to the y axis, the maximal velocity V_{smax} can be extracted from these profiles. It turns out that the maximal velocity is roughly located at a distance $y = \delta$ from the tip.

A more careful examination of the decaying of $V_s(x = 0, y)$ suggests that the influence of viscosity is mainly significant within the region of a few VBLs in thickness. Conversely, the decaying zone further from the tip seems to follow a decreasing exponential behaviour, which is almost independent of ν: the profiles are just shifted from each other by a velocity offset. In addition, at a distance of roughly 130 μm, $V_s(x = 0, y)$ approaches zero for all cases. This length scale seems to depend only on the sharp edge structure, which is in our case characterised by an angle of 60°, and tip height h = 180 μm.

Now we focus on the measurements obtained within a large range of V_a. Quantitatively, we mainly focus on the maximal and characteristic value of $V_s(x, y)$ measured around $y = \delta$ and at $x = 0$. In what follows, we shall also extract the prefactor θ that relates V_s to V_a^2, from the whole data set where the dependence is linear. Back to Equation (1), θ is equal to $\frac{1}{\nu} \frac{\delta^{2n-1}}{a^{2n-2}}$, from which the dependence on ν and on f can be readily predicted, taking $\alpha = 60°$ as in our experiments:

$$V_s \sim \nu^{-0.9} f^{-0.1} V_a^2 \tag{2}$$

To verify this theory, Figure 6 show the results of the experimental maximal streaming velocity $V_{s\,max}$ versus the square of the acoustic forcing velocity amplitude V_a^2, presented either as raw data (Left) or via the quantity $V_{s\,max} \times \nu^{-a}$, with a is an exponent deduced from Ovchinnikov et al.'s theory [37], equal to -0.9 for an angle $\alpha = 60°$ as stated above. In the inset, the quantity $V_{s\,max} \times \nu^{1/2}$ plotted versus V_a^2 shows a partial collapse of data in the range of the smallest values of V_a^2, roughly below 800 mm^2/s. At this stage of our investigations, we are unable to explain such a trend. From these results, we can simply conclude that viscosity strongly influences the streaming flow generated around sharp edges. But the dependence cannot be simply captured by the predictions of the perturbative theory from Ovchinnikov et al. [37], nor by any arbitrary power-law. In any case, the results show the quantitative confirmation that the independence on ν observed in classical Rayleigh–Schlichting streaming is lost in sharp-edge streaming.
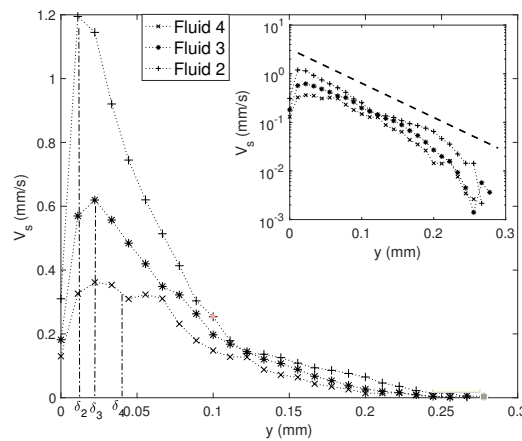

Figure 5. Streaming velocity profile along vertical direction $V_s(y)$, for three different viscosities (Fluids 2, 3 and 4 with ν respectively equal to 1.158, 4.32 and 13.75 mm^2/s). The operation condition is at frequency f = 2500 Hz and acoustic velocity V_a = 35 mm/s. Additionally labelled are the values of the VBL thickness for the three fluids δ_2, δ_3 and δ_4. The inset plots the same data in Lin-log axes.
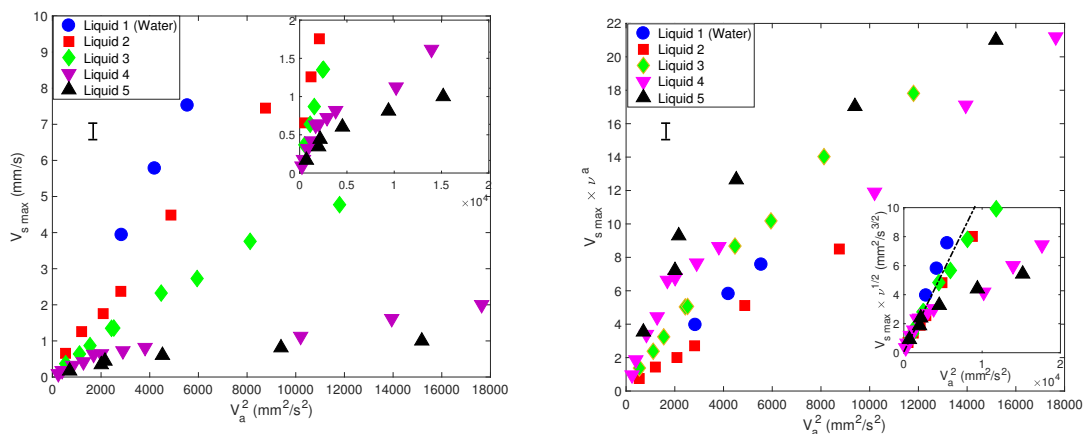

Figure 6. Left —Maximal streaming velocity $V_{s\,max}$ versus the square of the acoustic forcing velocity V_a^2, for different liquid viscosities ν, indicated in Table 2. Right—Quantity $V_{s\,max} \times \nu^{-a}$, with a= -0.9. Inset $V_{s\,max} \times \nu^{1/2}$. All measurements were obtained at f = 2500 Hz. The averaged typical error bar is indicated.

Let us finally point out that for more viscous liquids (4 and 5), there is a clear departure from a linear dependence between V_{smax} and V_a^2, typically as V_a^2 is larger than roughly 800 mm^2/s. For these two liquids, at 2500 Hz, δ_4 = 41.8 μm and δ_5 = 61.2 μm; hence, p^* is of the order of one.

4. Influence of Frequency

4.1. Velocity and Vorticity Maps

Figure 7a–d presents typical streaming velocity fields at different frequencies (f = 3500, 2500, 1250 and 800 Hz) with the same liquid viscosity (ν = 4.32 mm^2/s) and forcing amplitude (V_a = 22.4 mm/s). The same global structure with the main central jet and the inner and outer vortices are observed for all frequencies. The frequency does not seem to significantly influence the order of magnitude of the flow. Figure 8a–d shows the corresponding vorticity maps. Let us note that the colourmap scale is comparable for all four frequencies. As frequency gets lower, one observes a thicker and more intense inner VBL along the walls, while the outer vortices are more spread. The magnitude of vorticity in the outer vortices does not vary much with f.
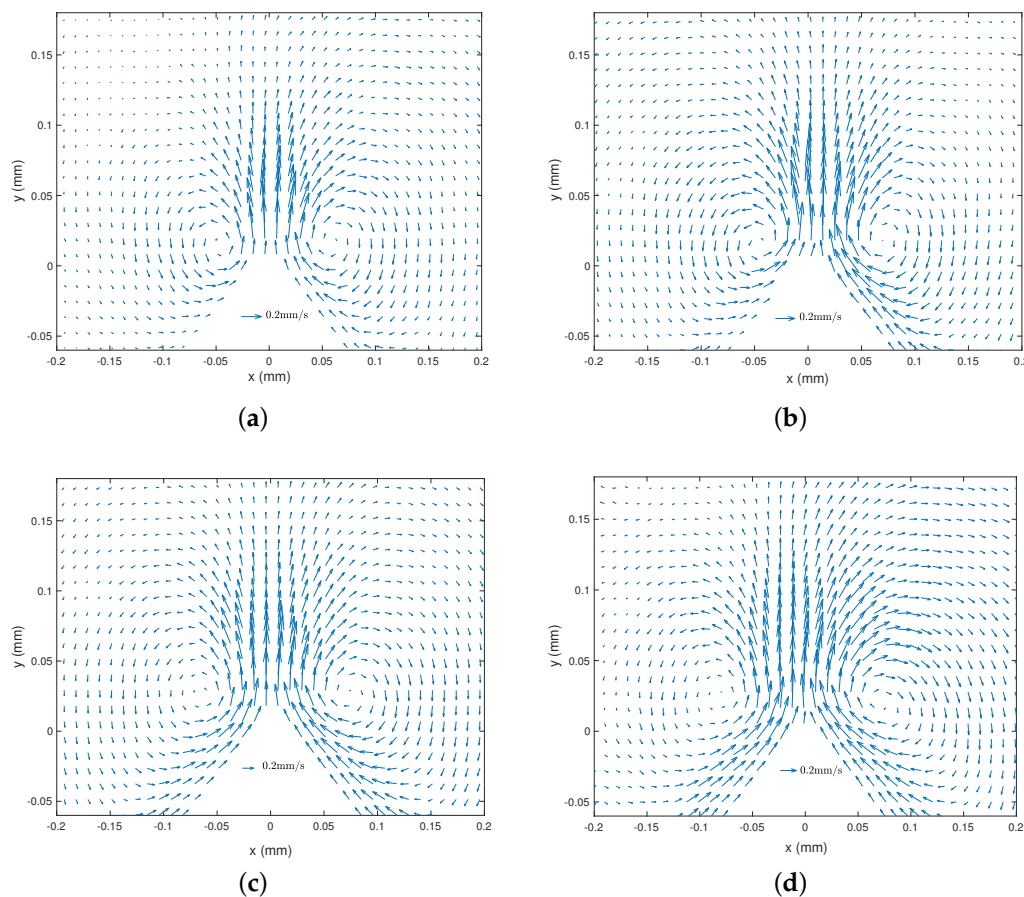

(a)

(b)

(c)

(d)

Figure 7. Streaming velocity field $V_s(x, y)$ from PIV measurements, with different excitation frequencies ν = 4.32 mm^2/s (Fluid 3) and V_a = 22.4 mm/s. (**a**) f = 3500 Hz, (**b**) f = 2500 Hz, (**c**) f = 1250 Hz, (**d**) f = 800 Hz. Scales are the same for the four cases.
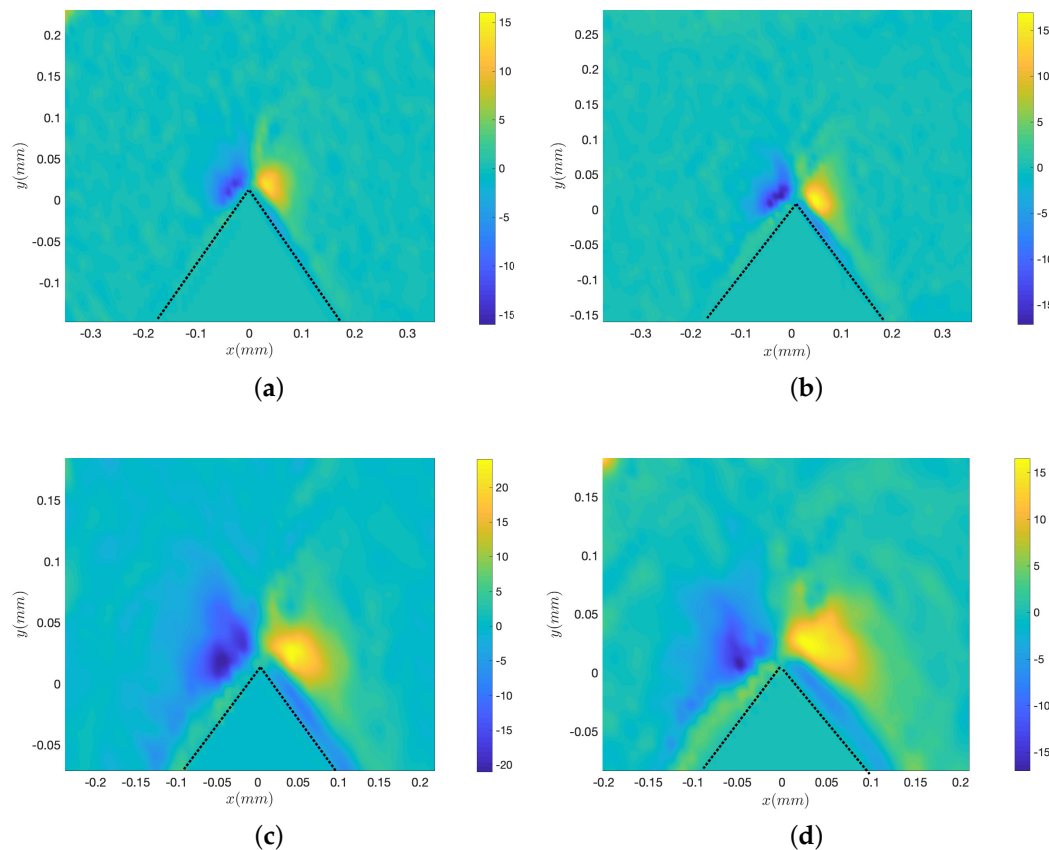
Figure 8. Vorticity maps of the streaming fields corresponding to the cases of Figure 7a–d. $\nu = 4.32$ mm^2/s (Fluid 3) and $V_a = 22.4$ mm/s. (**a**) $f = 3500$ Hz, (**b**) $f = 2500$ Hz, (**c**) $f = 1250$ Hz, (**d**) $f = 800$ Hz. Dotted lines show the boundaries of the sharp edge.

4.2. Maximal Velocity at Different Frequencies

We extract the velocity profile $V_s(x = 0, y)$ for the four values of frequency, under the same conditions as those of Figures 7 and 8; in particular, V_a is fixed at 22 mm/s. Results are plotted in Figure 9. The y locations of the maxima roughly correspond to the VBL thickness at respective f: $\delta_{3500} \simeq 19.8$ µm, $\delta_{2500} \simeq 23.4$ µm, $\delta_{1250} \simeq = 33.2$ µm and $\delta_{800} \simeq 41.5$ µm. The maximal velocity itself is very much dependent on f, but the typical length-scale of the decay along y is comparable for all four experiments, as revealed by the Lin-log plot in the insert. The four velocity profiles are shifted from each other with a given offset.

Figure 10 shows the maximal velocity $V_{s\,\text{max}}$ versus the square of the acoustic forcing velocity V_a^2, for different values of frequencies f and the same liquid viscosity $\nu = 4.32$ mm^2/s. Each data group obtained at constant f shows a linear trend: $V_{s\,\text{max}} = \theta V_a^2$. However, the dependence of the prefactor θ on f is unclear. Obviously, the theoretical prediction of [37] shown in Equation (2) fails to predict this strong dependence on f. However, it is possible to make two groups of data:

-   One group rather concerns measurements obtained at higher frequencies (2500 and 3500 Hz) and high V_a, for which a good fit is obtained for a value $\theta = 5 \times 10^{-4}$ s/mm.
-   The other group is constituted by measurements obtained at lower frequencies (500, 800 and 1250 Hz) and relatively low V_a; see insert in Figure 10. In this case, the value of the prefactor is $\theta = 0.0011$ s/mm.

To further test the possibility of a scaling law that would capture the dependence of the streaming velocity on f, we attempted to plot $V_{s\,\text{max}}$ versus potential pertinent combinations of

powers of V_a and f. In classical Rayleigh–Schlichting streaming, $V_{s\,max}$ usually depends linearly on $A^2 f = V_a^2/(4\,\pi^2\,f)$ [42,45]. But it turns out that plotting $V_{s\,max}$ versus $V_a^2/(4\pi^2 f)$ leads to even more scattered data points.

In seeking an empirical law quantifying the dependence on f, we then tried to plot V_s versus other combinations of V_a^2 and f^β, with β being a real exponent, predicted to equal -0.1 from Ovchinnikov et al.'s theory [37]; see Equation (2). Figure 11 show the two most successful attempts:

- Figure 11a: the plot of V_s versus $V_a^2 \times f$ shows a good collapse of data for the three lowest frequency values (500, 800 and 1250 Hz). But the rescaling does not fit with the two other data sets corresponding to the highest frequencies (2500 and 3500 Hz).
- Figure 11b: the plot of V_s versus $V_a^2 \times f^{-1/2}$ shows a fair collapse of data for all frequencies, though it is more convincing at higher acoustic amplitude.
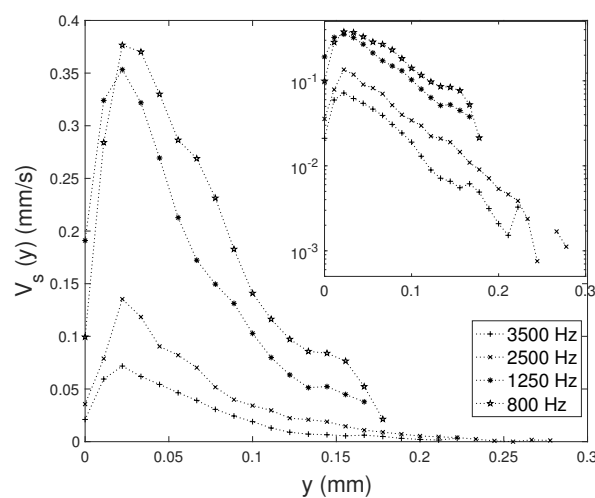

Figure 9. Streaming velocity profile along vertical direction $V_s(y)$, for four different frequencies. Liquid viscosity $\nu = 4.32$ mm^2/s and $V_a = 22$ mm/s. The inset plots the same data in Lin-log axes.
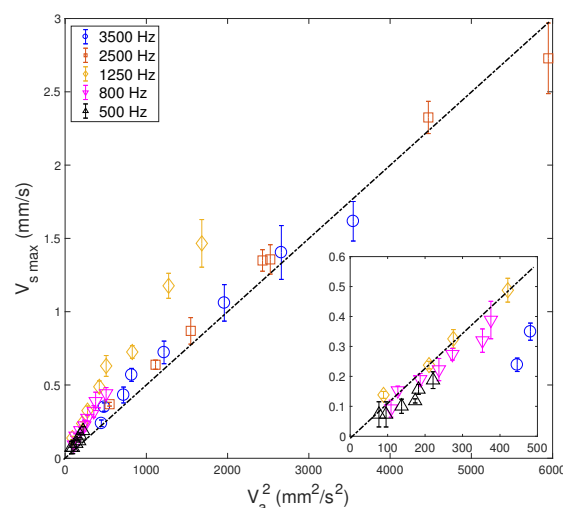

Figure 10. Maximal streaming velocity $V_{s\,max}$ versus V_a^2, for different f and the same viscosity $\nu = 4.32$ mm^2/s. The dashed-dotted line suggests a linear relationship, with a prefactor $\theta = 5\times10^{-4}$ s/mm. The inset represents a magnified view of the plot for the lowest values of V_a^2, suggesting a linear scaling with a prefactor $\theta = 0.0011$ s/mm.
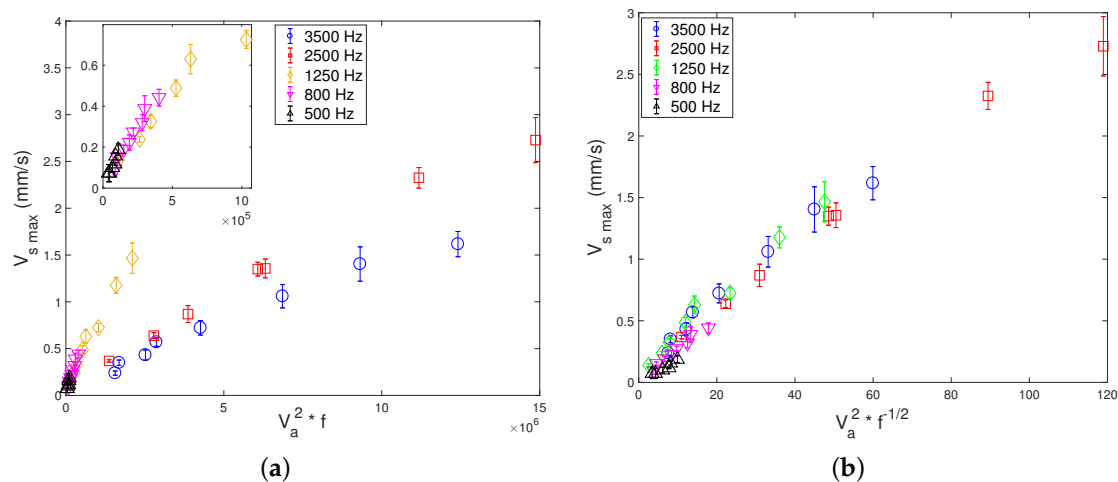
Figure 11. Attempts of data rescalling for $V_{s\,max}$ (**a**) versus $V_a^2 \times f$ (insert shows data in the lowest range of V_a^2) and (**b**) versus $V_a^2 \times f^{-1/2}$ showing a fair collapse of data.

Still, there is no clear explanation for such trends. Therefore, it is likely that the dependence of the streaming flow on f cannot be captured by simple theoretical predictions.

5. Conclusions

Our study presents qualitative and quantitative results of the streaming flow generated by long-wavelength/low-frequency acoustic fields near a sharp-edge. The main focus has been given to viscosity (ν from pure water to 30 times higher), with frequency f from 500 to 3500 Hz, allowing us to tune the VBL thickness δ from 9.5 to 137 μm. The mechanisms of such a streaming flow, described in previous studies [30–35,37], are distinct from those of the classical Rayleigh–Schlichting streaming. Our results confirm a strong link of sharp-edge streaming to viscosity and frequency. But the dependency on both ν and f seems to be more complex than simple power law descriptions; for instance, those from Ovchinnikov et al.'s study [37]. Let us mention a very recent study [34] where streaming velocity is predicted analytically and numerically. Equations (27)–(28) and (37)–(38) in [34] offer a complete prediction, including the structure of the flow itself. By comparing the scaling laws from this study with our experiments, we could not find agreement. We assume the complex behaviour in our experiments is due to the fact that δ can become comparable to the channel depth. Therefore, we hope our results will provide an interesting challenge for future studies involving complex geometries.

Still, our results allow one to draw several conclusions:

- For any conditions, the maximal streaming velocity is roughly located at a vertical distance of δ from the tip; i.e., just at the limit of the VBL.
- An increase of viscosity leads to globally weaken the streaming velocity and the outer vorticity. Still, the outer vortices keep their size and shape for all liquids, and the thickness of the inner flow along the edge lateral walls roughly remains insensitive to viscosity. This is clearly at odds from what is observed in classical boundary-layer (Rayleigh–Schlichting) streaming.
- At constant V_a, a decrease of frequency tends to increase the streaming velocity. Our results, although unexplained by the current theoretical state of the art, suggests the empirical law: $V_s \sim V_a^2 f^{-1/2}$. Furthermore, the lower the frequency f is, the more spread out the streaming vortices are.
- While the flow near the tip ($r < \delta$) is strongly influenced by ν and f, the flow far from the tip follows an exponential decrease over a length scale of roughly 130 μm, under the test condition and with angle of 60°, and tip height $h = 180$ μm. This length characterises the disturbance distance and seems to be dependent only on the sharp edge structure rather than the operating conditions.

- When the VBL thickness is comparable to the channel depth, i.e., when p^* is of the order one, the dependence of V_{smax} on V_a^2 is no longer linear. It suggests that $p^* \gg 1$ is a necessary condition for this linearity, as otherwise the streaming flow cannot fully develop within the channel.

Author Contributions: X.G., L.R. and P.B. planned the work. C.Z. and P.B. fabricated the device. C.Z. carried out the experiments. C.Z., X.G., L.R. and P.B. discussed the results and their presentation in figures. P.B. wrote the first draft of the paper. C.Z., X.G., L.R. and P.B. wrote the paper. All authors have read and agreed to the published version of the manuscript.

Conflicts of Interest: The authors declare no conflict of interest.

Abbreviations

The following abbreviations are used in this manuscript:

VBL   Viscous boundary layer

References

1. Westervelt, P.J. The Theory of Steady Rotational Flow Generated by a Sound Field. *J. Acoust. Soc. Am.* **1953**, *25*, 60–67. doi:10.1121/1.1907009.
2. Nyborg, W.L. Acoustic Streaming due to Attenuated Plane Waves. *J. Acoust. Soc. Am.* **1953**, *25*, 68–75. doi:10.1121/1.1907010.
3. Lighthill, S.J. Acoustic Streaming. *J. Sound Vib.* **1978**, *61*, 391–418.
4. Friend, J.; Yeo, L.Y. Microscale acoustofluidics: Microfluidics driven via acoustics and ultrasonics. *Rev. Mod. Phys.* **2011**, *83*, 647.
5. Eckart, C. Vortices and streams caused by sound waves. *Phys. Rev.* **1948**, *73*, 68–76. doi:10.1103/PhysRev.73.68.
6. Rayleigh, L. On the circulation of air observed in Kundt's tubes, and on some allied acoustical problems. *Philos. Trans. R. Soc. Lond.* **1884**, *175*, 1–21.
7. Schlichting, H.; Gersten, K. *Boundary-Layer Theory*; Springer Nature: Berlin, Germany, 2017.
8. Nyborg, W.L. Acoustic Streaming near a Boundary. *J. Acoust. Soc. Am.* **1958**, *30*, 329–339. doi:10.1121/1.1909587.
9. Riley, N. *Acoustic Streaming*; Springer US: Boston, MA, USA, 1998; Volume 10, pp. 349–356. doi:10.1007/s001620050068.
10. Rayleigh, L. *The Theory of Sound, Volume One*; Dover Publications: New York, NY , USA, 1945; p. 985.
11. Faraday, M. On a Peculiar Class of Acoustical Figures; and on Certain Forms Assumed by Groups of Particles upon Vibrating Elastic Surfaces. *Philos. Trans. R. Soc. Lond.* **1831**, *121*, 299–340. doi:10.1098/rstl.1831.0018.
12. Sritharan, K.; Strobl, C.J.; Schneider, M.F.; Wixforth, A. Acoustic mixing at low Reynold's numbers. *Appl. Phys. Lett.* **2006**, *88*, 054102.
13. Franke, T.; Braunmuller, S.; Schmid, L.; Wixforth, A.; Weitz, D.A. Surface acoustic wave actuated cell sorting (SAWACS). *Lab Chip* **2010**, *10*, 789–794.
14. Lenshof, A.; Magnusson, C.; Laurell, T. Acoustofluidics 8: Applications ofacoustophoresis in continuous flowmicrosystems. *Lab Chip* **2012**, *12*, 1210.
15. Sadhal, S.S. Acoustofluidics 15: Streaming with sound waves interacting with solid particles. *Lab Chip* **2012**, *12*, 2600. doi:10.1039/c2lc40243b.
16. Muller, P.B.; Rossi, M.; Marin, A.G.; Barnkop, R.; Augustsson, P.; Laurell, T.; Kahler, C.J.; Bruus, H. Ultrasound-induced acoustophoretic motion of microparticles in three dimensions. *Phys. Rev. E* **2013**, *88*, 023006.
17. Skov, N.R.; Sehgal, P.; Kirby, B.J.; Bruus, H. Three-Dimensional Numerical Modeling of Surface-Acoustic-Wave Devices: Acoustophoresis of Micro-and Nanoparticles Including Streaming. *Phys. Rev. Appl.* **2019**, *12*, 044028. doi:10.1103/PhysRevApplied.12.044028.

18. Qiu, W.; Karlsen, J.T.; Bruus, H.; Augustsson, P. Experimental Characterization of Acoustic Streaming in Gradients of Density and Compressibility. *Phys. Rev. Appl.* **2019**, *11*, 024018. doi:10.1103/PhysRevApplied.11.024018.

19. Voth, G.A.; Bigger, B.; Buckley, M.R.; Losert, W.; Brenner, M.P.; Stone, H.A.; Gollub, J.P. Ordered clusters and dynamical states of particles in a vibrated fluid. *Phys. Rev. Lett.* **2002**, *88*, 234301.

20. Vuillermet, G.; Gires, P.Y.; Casset, F.; Poulain, C. Chladni Patterns in a Liquid at Microscale. *Phys. Rev. Lett* **2016**, *116*, 184501.

21. Legay, M.; Simony, B.; Boldo, P.; Gondrexon, N.; Le Person, S.; Bontemps, A. Improvement of heat transfer by means of ultrasound: Application to a double-tube heat exchanger. *Ultrason. Sonochem.* **2012**, *19*, 1194–1200. doi:10.1016/J.ULTSONCH.2012.04.001.

22. Loh, B.G.; Hyun, S.; Ro, P.I.; Kleinstreuer, C. Acoustic streaming induced by ultrasonic flexural vibrations and associated enhancement of convective heat transfer. *J. Acoust. Soc. Am.* **2002**, *111*, 875–883.

23. Kamakura, T.; Sudo, T.; Matsuda, K.; Kumamoto, Y. Time evolution of acoustic streaming from a planar ultrasound source. *J. Acoust. Soc. Am.* **1996**, *100*, 132–138.

24. Brunet, P.; Baudoin, M.; Bou Matar, O.; Zoueshtiagh, F. Droplet displacements and oscillations induced by ultrasonic surface acoustic waves: A quantitative study. *Phys. Rev. E* **2010**, *81*, 036315.

25. Moudjed, B.; Botton, V.; Henry, D.; Ben Hadid, H.; Garandet, J.P. Scaling and dimensional analysis of acoustic streaming jets. *Phys. Fluids* **2014**, *26*, 093602.

26. Da Costa Andrade, E.N. On the circulations caused by the vibration of air in a tube. *Proc. R. Soc.* **1931**, *134*, 445.

27. Valverde, J.M. Pattern-formation under acoustic driving forces. *Contemp. Phys.* **2015**, *56*, 338–358.

28. Hamilton, M.F.; Ilinskii, Y.A.; Zabolotskaya, E. Acoustic streaming generated by standing waves in two-dimensional channels of arbitrary width. *J. Acoust. Soc. Am.* **2002**, *113*, 153–160.

29. Wiklund, M.; Green, R.; Ohlin, M. Acoustofluidics 14: Applications of acoustic streaming in microfluidic devices. *Lab Chip* **2012**, *12*, 2438. doi:10.1039/c2lc40203c.

30. Huang, P.H.; Xie, Y.; Ahmed, D.; Rufo, J.; Nama, N.; Chen, Y.; Chan, C.Y.; Huang, T.J. An acoustofluidic micromixer based on oscillating sidewall sharp-edges. *Lab Chip* **2013**, *13*, 3847–3852. doi:10.1039/c3lc50568e.

31. Huang, P.H.; Nama, N.; Mao, Z.; Li, P.; Rufo, J.; Chen, Y.; Xie, Y.; Wei, C.H.; Wang, L.; Huang, T.J. A reliable and programmable acoustofluidic pump powered by oscillating sharp-edge structures. *Lab Chip* **2014**, *14*, 4319–4323.

32. Nama, N.; Huang, P.H.; Huang, T.J.; Costanzo, F. Investigation of acoustic streaming patterns around oscillating sharp edges. *Lab Chip* **2014**, *14*, 2824–2836.

33. Nama, N.; Huang, P.H.; Huang, T.J.; Costanzo, F. Investigation of micromixing by acoustically oscillated sharp-edges. *Biomicrofluidics* **2016**, *10*, 024124.

34. Doinikov, A.A.; Gerlt, M.S.; Pavlic, A.; Dual, J. Acoustic streaming produced by sharp-edge structures in microfluidic devices. *Microfluid. Nanofluid.* **2020**, *24*, 32.

35. Zhang, C.; Guo, X.; Brunet, P.; Costalonga, M.; Royon, L. Acoustic streaming near a sharp structure and its mixing performance characterization. *Microfluid. Nanofluid.* **2019**, *23*, 104. doi:10.1007/s10404-019-2271-5.

36. Zhang, C.; Guo, X.; Royon, L.; Brunet, P. Unveiling of the mechanisms of acoustic streaming induced by sharp edges. *arXiv* **2020**, arXiv:2003.01208.

37. Ovchinnikov, M.; Zhou, J.; Yalamanchili, S. Acoustic streaming of a sharp edge. *J. Acoust. Soc. Am.* **2014**, *136*, 22–29. doi:10.1121/1.4881919.

38. Huang, P.H.; Chan, C.Y.; Li, P.; Wang, Y.; Nama, N.; Bachman, H.; Huang, T.J. A sharp-edge-based acoustofluidic chemical signal generator. *Lab Chip* **2018**, *18*, 1411–1421. doi:10.1039/C8LC00193F.

39. Leibacher, I.; Hahn, P.; Dual, J. Acoustophoretic cell and particle trapping on microfluidic sharp edges. *Microfluid. Nanofluid.* **2015**, *19*, 923–933. doi:10.1007/s10404-015-1621-1.

40. Cao, Z.; Lu, C. A Microfluidic Device with Integrated Sonication and Immunoprecipitation for Sensitive Epigenetic Assays. *Anal. Chem.* **2016**, *88*, 1965–1972. doi:10.1021/acs.analchem.5b04707.

41. Bachman, H.; Huang, P.H.; Zhao, S.; Yang, S.; Zhang, P.; Fu, H.; Huang, T.J. Acoustofluidic devices controlled by cell phones. *Lab Chip* **2018**, *18*, 433–441. doi:10.1039/C7LC01222E.

42. Costalonga, M.; Brunet, P.; Peerhossaini, H. Low frequency vibration induced streaming in a Hele-Shaw cell. *Phys. Fluids* **2015**, *27*, 013101.

43. Cheng, N.S. Formula for the viscosity of a glycerol-water mixture. *Ind. Eng. Chem. Res.* **2008**, *47*, 3285–3288.

44.   Slie, W.M.; Donfor, A.R.; Litovitz, T.A. Ultrasonic shear and longitudinal measurements in aqueous glycerol. *J. Chem. Phys.* **1966**, *44*, 3712–3718.

45.   Bahrani, S.; Perinet, N.; Costalonga, M.; Royon, L.; Brunet, P. Vortex elongation in outer streaming flows. *Exp. Fluids* **2020**, *61*, 91.